

Tyrosyl Fluorescence Decays and Rotational Dynamics in Tyrosine Monomers and in Dipeptides

Greg S. Harms,¹ Steve W. Pauls,¹ John F. Hedstrom,² and Carey K. Johnson^{1,3}

Received August 22, 1997; revised December 3, 1997; accepted December 29, 1997

Picosecond time-correlated single-photon counting was used to measure fluorescence lifetimes and fluorescence anisotropy decays of tyrosine and the tyrosine-alanine and tyrosine-leucine dipeptides. After excitation of tyrosine at 287 nm two emitting species were observed, one at 303 nm with a lifetime of 3.3 ns and another at 340 nm with a lifetime of 360 ps. The rotational correlation time of tyrosine at 303 nm is 38 ps in water at pH 7 and depends linearly on viscosity with a slope of 44 ps/cP, consistent with Stokes-Einstein-Debye theory. We calculated a value of 45 ns for the radiative lifetime of tyrosine, yielding a fluorescence quantum yield of 0.07. The dipeptides Tyr-Ala and Tyr-Leu exhibit two- or three-exponential decays. The amplitudes of the decay components for three-exponential fits correlate closely with the populations of rotamers in these peptides as determined by NMR. The quenching of dipeptide fluorescence is shown to depend on the solvent polarity, strongly supporting the hypothesis that tyrosyl fluorescence in peptides is quenched by charge transfer. The rotational correlation times of tyrosine, Tyr-Ala, and Tyr-Leu increase linearly with the van der Waals volumes. However, rotational relaxation is somewhat faster than expected from Stokes-Einstein-Debye theory with "stick" boundary conditions.

KEY WORDS: Tyrosine; dipeptides; time-correlated single-photon counting; fluorescence intensity; rotamers; fluorescence anisotropy; rotational correlation times.

INTRODUCTION

Over the past two decades, fluorescence has become a valuable tool in investigations of the physical properties of biomolecules.⁽¹⁾ Studies of the fluorescence of biomolecules provide information on the structure and conformational motions of peptides and proteins not available from X-ray diffraction and NMR techniques. Fluorescence measurements offer the advantages of time resolution and superior sensitivity, requiring smaller sample volumes and lower concentrations for detection. Enhanced time resolution, which has been made possible

by advances in ultrashort laser pulses, opens a window onto the time regime spanned by molecular dynamics simulations of the conformational motions of peptides and proteins. Thus, fluorescence and rotational diffusion studies combined with molecular dynamics simulations can provide powerful insights into dynamics of peptides and proteins.

The fluorescence decay properties of tyrosine have been investigated in a number of laboratories.⁽²⁻⁷⁾ Nevertheless, in contrast to tryptophan, the fluorescence of tyrosine remains largely unexploited due in part to its low absorption cross section and low fluorescence quantum yield. However, with the availability of high-power UV laser sources and increased detector sensitivity, fluorescence studies of tyrosine in biological systems have begun to flourish during the past decade.⁽⁷⁾ An added advantage of probing tyrosine fluorescence is that the

¹ Department of Chemistry, University of Kansas, Lawrence, Kansas 66045.

² Department of Chemistry, Luther College, Decorah, Iowa 52101.

³ To whom correspondence should be addressed. e-mail: cjohnson@eureka.chem.ukans.edu. Fax: 785-864-5396.

initial anisotropy in the L_b state is quite high,^(3,8,9) facilitating studies of rotational and conformational dynamics in biological systems. The initial anisotropy of tyrosine has been reported to be as high as about 0.3 in aqueous solutions at 25°C.^(3,9) However, only one other source has previously reported the rotational correlation time of free L-tyrosine under these conditions.⁽³⁾

Although reports generally agree about the approximate fluorescence lifetimes of free tyrosine,^(2,4,6,7,10–12) several explanations have been offered for the underlying mechanistic causes of fluorescence quenching in tyrosine. These include proton transfer, intersystem crossing, internal conversion, and charge transfer. A compelling explanation is based on the rotamer model, which relates multiexponential fluorescence decays in peptides and proteins to populations of three rotamers with different dihedral angles (χ^1) about the C^α – C^β side-chain bond.^(2,10) Evidence from solution NMR indicates that distinct populations of rotamers exist.^(5,10,13) An alternative view considers the conformations described by the dihedral angles ϕ and θ between the α carbon of tyrosine and the peptide chain.⁽¹¹⁾

The rotamer model attributes quenching to charge transfer interactions with nearby groups. Multiexponential fluorescence decays of tyrosine then reflect different quenching rates that depend on the tyrosine environment.^(7,10) Fluorescence quenching in peptides via charge transfer has been described by Cowgill^(14,15) and by Seidel *et al.*⁽¹⁶⁾ In this picture, weakly electron withdrawing amide groups and opposing electron-donating groups such as carboxylate regulate the charge-transfer quenching of tyrosine by the electron-withdrawing peptidic ammonium group. Interactions of tyrosine with other ionizable amino acid groups such as arginine, lysine, and histidine also have appreciable effects on the fluorescence of tyrosine.⁽¹⁵⁾

Fluorescence quenching is also reflected in the fluorescence quantum yield. However, discrepancies exist in the reported fluorescence quantum yield of tyrosine itself. The quantum yield has been reported to be as high as 0.21⁽¹⁷⁾ and as low as 0.04.⁽¹⁸⁾ Some differences in reported values may result because the quantum yield is naturally dependent on conditions such as temperature, solvent, absorption and emission wavelength, and pH. However, discrepancies remain in the fluorescence quantum yield of tyrosine.

We have recently initiated experiments with tyrosine fluorescence as an intrinsic probe of dynamics in biological systems. In this paper, we report fluorescence lifetimes, rotational times, and quantum yields for tyrosine, tyrosine–alanine, and tyrosine–leucine. Our intent is to understand the time-dependent properties of the flu-

orescence of tyrosine and tyrosine-containing dipeptides as a foundation for further fluorescence studies of tyrosine in peptides and proteins. We focus on several key aspects of tyrosine fluorescence: intrinsic fluorescence decay times and quantum yields, quenching mechanisms, and the correlation between rotamer populations and multiexponential decays. Then, we examine the nature of fluorescence anisotropy decay in tyrosine and in dipeptides. We show that anisotropy decays can provide valuable information regarding the identity of the fluorescing species. In the following paper we report a study of fluorescence from dityrosine.⁽¹⁹⁾

MATERIALS AND METHODS

Chemicals and Preparations

L-Tyrosine, tyrosine–alanine, tyrosine–leucine, and *p*-cresol were purchased from Sigma and were checked for purity by HPLC. The samples were all dissolved in either Nanopure water adjusted for pH (by the addition of 0.1 M HCl or 0.1 M NaOH) or 10 mM phosphate buffer prepared from Nanopure water. For viscosity-dependent studies, solutions of tyrosine were prepared in octanol, ethylene glycol/water, propylene glycol/water, and glycerol/water mixtures. Concentrations of tyrosine and *p*-cresol were 100 to 500 μ M. Concentrations of tyrosine dipeptides were 70 to 100 μ M. All solutions were bubbled with argon for at least 10 min with a slow gas flow to deoxygenate them prior to use.

Experimental Setup

The fluorescence excitation pulse was provided by a cavity-dumped rhodamine-590 dye laser, which was synchronously pumped by the second harmonic from a Coherent Antares Nd:YAG laser. The pulse repetition rate of the dye laser was 3.975 MHz, with a half-width of about 5 ps and an average power of 250 mW. These pulses were frequency-doubled by a BBO crystal to provide an excitation wavelength of 287 nm. The excitation beam was focused onto the sample by a 10-cm lens. The focal point was set near the front face of a 1.0 \times 1.0-cm quartz sample cell to minimize reabsorption. The fluorescence was then collected by an off-axis ellipsoidal mirror (Janos Technology) at a right-angle configuration. Emission photons were passed through a polarizer followed by a polarization scrambler and focused into a small double holographic monochromator (American Holographic DB-10). After emerging from the monochromator the emission was focused onto a chilled MCP-

PMT tube (Hamamatsu R3809U). Temperature control of the sample cell was provided by flowing a coolant (ethylene glycol) through a homemade sample cell holder.

The fluorescence signal was processed by time-correlated single-photon counting (TCSPC) instrumentation consisting of a constant-fraction discriminator (Oxford), time-to-amplitude converter (TAC) (Tennelek), and multichannel analyzer (Nucleus). The TCSPC instrument was operated in reverse mode,⁽²⁰⁾ where the TAC is started by a fluorescence count and stopped by a reference signal that is generated by a small portion of the excitation pulse that was delayed in an optical fiber.

Data Collection and Fitting

For each fluorescence decay experiment, the instrument response function was obtained after data collection by monitoring the scattering of the excitation pulse from a dilute solution of nondairy creamer. The FWHM of the instrument response was of the order of about 20 ps. The instrument function was always collected to the same maximum number of counts as the peak channel of the fluorescence decay data.

Fluorescence depolarization measurements were obtained by collection of fluorescence polarized parallel and perpendicular to the vertical excitation polarization. The anisotropy decay, $r(t)$, was determined by simultaneously fitting the parallel and perpendicular components, I_{\parallel} and I_{\perp} .⁽²¹⁾ A factor g was used to correct for any difference in efficiency of collection of parallel (I_{\parallel}) and perpendicular (I_{\perp}) fluorescence polarization. The correction factor g was obtained from the ratio of fluorescence intensities with horizontal and vertical polarization measured with horizontal excitation polarization. The corrected anisotropy is given by

$$r = \frac{I_{\parallel} - gI_{\perp}}{I_{\parallel} + 2gI_{\perp}} \quad (1)$$

The value of g factor varied from 1.002 to about 1.009, with an average value of about 1.007. Isotropic intensity decays (I_{MA}) were measured independent of rotational motion by setting the emission polarizer to the magic angle, 54.7° from vertical.

We analyzed the fluorescence decays, I_{MA} , I_{\parallel} , and I_{\perp} , with fitting programs generously shared by Prof. Graham Fleming and Dr. Gary Holtom. Fluorescence lifetime fits to I_{MA} were obtained with the fitting function $K(t) = \sum a_i \exp(-t/\tau_i)$, with $i = 1$ to 4. To determine the anisotropy and rotational correlation times accurately, we first determined the $K(t)$ population decay

parameters from multiple measurements with the analyzing polarizer at the magic angle. Fitting parameters were optimized by nonlinear least-squares fitting using the Levenberg–Marquardt algorithm with iterative convolution. The quality of the fit, $F(t)$, was judged by the reduced χ^2 defined by

$$\chi^2 = \sum [I_i(t) - F_i(t)]^2 / (\nu \sigma_i^2) \quad (2)$$

where σ is the standard deviation and ν is the number of degrees of freedom. In most cases, optimized fitting parameters for the population decay function $K(t)$ obtained from fits to I_{\parallel} and I_{\perp} were nearly identical to those obtained from magic-angle fits. For the few exceptions, fits to $I_{\parallel}(t)$ and $I_{\perp}(t)$ were obtained with the $K(t)$ parameters fixed to values obtained previously from magic-angle measurements.

Determination of Radiative Lifetimes

Radiative lifetimes were calculated by the method of Strickler and Berg⁽²²⁾ as modified by Birks and Dyson.⁽²³⁾ This method is based on the relationship between the radiative lifetime and the integrated absorption spectrum:

$$1/\tau_0 = 2.880 \times 10^{-9} n_r^3/n_a \langle \omega_r^{-3} \rangle_{AV}^{-1} \int \epsilon(\omega) d\ln\omega \quad (3)$$

where n_r and n_a are the refractive indices of the solution at the emission and absorption wavelengths, taken from the *International Critical Tables*,⁽²⁴⁾ ω is the wavenumber of absorption, ω_r is the emission wavenumber, and $\epsilon(\omega)$ is the wavenumber dependent absorption extinction coefficient. Absorption spectra were taken with a UVKON spectrophotometer (KONTRON Instruments, Type 99-09410). Emission spectra were recorded on a PTI fluorimeter. The absorption spectra were fit with a spectral fitting program to multiple Gaussians to obtain an expression for $\epsilon(\omega)$. The average $\langle \omega_r^{-3} \rangle_{AV}^{-1}$ was calculated by fitting the fluorescence spectra to five Gaussian functions and then calculating

$$\frac{\int I(\omega) d\omega}{\int \omega^{-3} I(\omega) d\omega} = \langle \omega_r^{-3} \rangle_{AV}^{-1} \quad (4)$$

The fluorescence quantum yield was calculated as $Q = \tau_F/\tau_0$, where $\tau_F = \sum b_i \tau_i$ is the average fluorescence lifetime.

NMR Measurement of Rotamer Populations

The rotamer populations of the tyrosine phenolic group were determined by the method of Ross and co-workers from the coupling constants between the H^{α} and

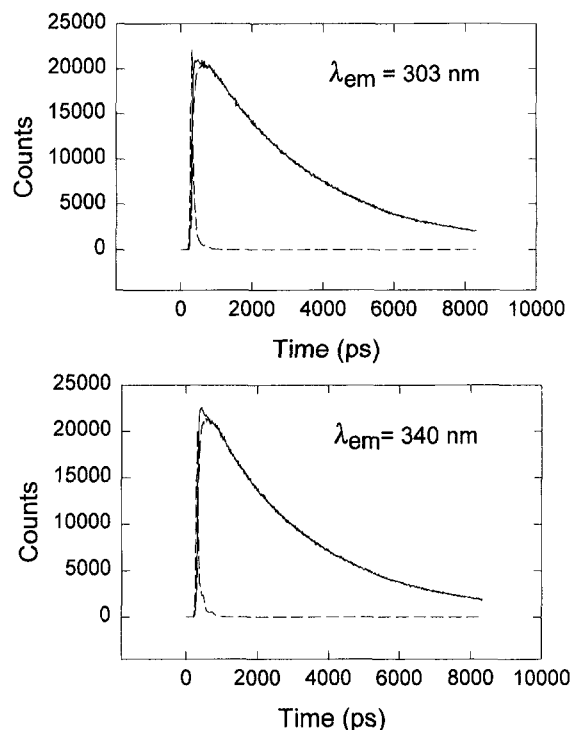


Fig. 1. Fluorescence decay profiles of tyrosine at 303 nm (top) and 340 nm (bottom) with excitation at 287 nm. Fluorescence anisotropy is apparent in the early portion of the decay. The upper curve shows the decay of fluorescence with polarization parallel to the excitation polarization, and the lower curve shows the decay of fluorescence with perpendicular polarization. Fluorescence intensity and anisotropy decay parameters are given in Table I.

the H^β protons.⁽¹⁰⁾ The tyrosine-alanine samples were dissolved in deuterated water or in deuterated acetonitrile. Concentrations were adjusted to 10 mM tyrosine-alanine. The NMR spectra were collected from the averaging of 16 scans on a Bruker 300 MHz NMR.

Solvent Polarity Dependence

Solvent polarity was varied by forming solutions with mixtures of nanopure water and acetonitrile. The solvent polarity of the mixtures was quantified by the $E_T(30)$ parameter determined by the method of Langhals.⁽²⁵⁾

RESULTS AND DISCUSSION

Fluorescence Intensity Decays

Figure 1 shows the parallel and perpendicular fluorescence decay components of tyrosine at pH 7 and

20°C with excitation at 287 nm and emission at 303 (top) and 340 nm (bottom). The 303-nm emission data fit well to a single-exponential fluorescence decay of 3.2 ± 0.1 ns, in good agreement with previous results.^(2-4,6,10) The emission data at 340 nm has two exponential components, with time constants of 3.1 (82%) and 0.36 ns (18%). The observation of two components at 340 nm has been reported previously.⁽²⁶⁾ The longer decay time corresponds closely to the time constant for tyrosine emission at 303 nm. The short decay component at 340 nm has been attributed to a hydrogen-bonded tyrosine complex.⁽²⁶⁾ The biexponential decay is consistent with the existence of two populations, one consisting of uncomplexed tyrosine, with a decay time of 3.1 ns, and the other consisting of complexed tyrosine, with a strongly quenched decay.

At pH values lower than 7, the emission at 303 nm could no longer be adequately fit with single-exponential decays. The fitting parameters for fluorescence decays of tyrosine at pH 2 to 10 are given in Table I. The data reported in Table I are averages of five or more scans for tyrosine in each solvent for the 303-nm emission data. The pH dependence, shown graphically in Fig. 2, follows the trend observed by Laws *et al.*⁽¹⁰⁾ The average fluorescence lifetime is about 3.0 ns, independent of pH between pH 4 and pH 10, but drops to 1.9 ns at pH 2. The fluorescence decays at pH 2 to pH 6 can be fit with two decay components, one of about 3 ns and the other of about 1.1 ns. These decay times are essentially invariant with pH. However, the corresponding amplitudes are pH dependent, with the amplitude of the shorter lifetime increasing as the pH is decreased. This behavior suggests a ground-state equilibrium with a pK_a that corresponds to that of the carboxylate group.

Fluorescence Quantum Yield

Fluorescence quantum yields were determined from the ratio $Q = \tau_F/\tau_0$ of the fluorescence and radiative lifetimes. The advantage of this approach over direct measurement of quantum yields is that it is not susceptible to contamination by scattered light and other uncertainties in direct quantum-yield measurements. The radiative lifetime τ_0 of tyrosine was determined by fitting and integrating the absorption and emission spectra, yielding $\tau_0 = 45$ ns. From the radiative lifetime and the measured fluorescence lifetime, the fluorescence quantum yield of tyrosine was calculated to be 0.07. Table II lists the quantum yield of tyrosine determined here and compares it to other previously reported values. The radiative lifetime from a similar calculation by Teale and Weber was 42 ns.⁽²⁷⁾ However, their value of the fluorescence quan-

Table I. Analysis of Tyrosine Fluorescence Decays

pH	λ_{em} (nm)	a_1	a_2	τ_1 (ns)	τ_2 (ns)	r_0	τ_{rot} (ps)	χ^2
2	303	0.59	0.41	1.24	2.81	0.29	71.3	2.9
4	303	0.22	0.78	1.06	3.52	0.29	75.0	2.0
6	303	0.15	0.85	1.08	3.45	0.29	51.0	2.0
7	303		1.0		3.16	0.29	37.7	1.3
8	303		1.0		3.31	0.29	37.2	1.3
10	303		1.0		3.12	0.29	37.5	1.5
7	340	0.18	0.82	0.36	3.10	0.18	47	1.6

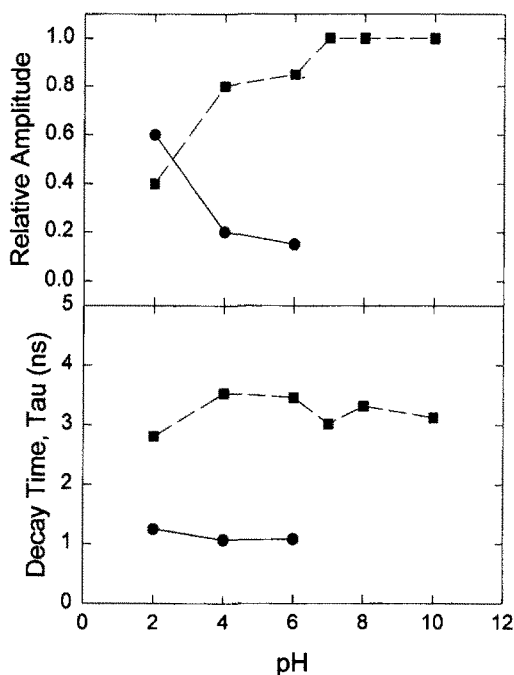


Fig. 2. Dependence of the tyrosine fluorescence decay parameters on pH. Fluorescence was excited at 287 nm and detected at 303 nm.

tum yield seems to be too large since it would predict that the fluorescence lifetime of tyrosine is 8 to 9 ns. Our calculated fluorescence quantum yield is similar to the value measured by Børresen.⁽²⁸⁾

Dipeptide Intensity Decays

Figures 3 and 4 depict decay data for tyrosine-alanine (YA) and tyrosine-leucine (YL) with excitation at 287 nm and emission at 303 and 340 nm. Fitting parameters are shown in Table III. The fluorescent decay times for both dipeptides with 303-nm emission and their average lifetimes (see Table III) of 1.4 ns for YA and YL are consistent with results reported by Gauduchon and

Wahl⁽²⁾ and Seidel *et al.*^(11,16) In general, the fluorescence decay times at 340 nm are not significantly changed from their 303-nm counterparts for the dipeptides.

In order to determine whether the multiexponential decays observed for the dipeptides are the result of subpopulations of rotamers about the χ_1 bond of tyrosine, rotamer populations for YA were determined by NMR. The results show that rotamers I, II, and III (see Table III) of YA in D₂O have the following relative populations: $p_I = 0.47$, $p_{II} = 0.33$, and $p_{III} = 0.20$. The 303-nm emission data yield a slightly improved fit with a three-exponential fit (see Table III). The three preexponential factors matched the rotamer populations within experimental error. In agreement with the results of Laws and Ross *et al.*⁽¹⁰⁾ for rotamer-linked populations for tyrosine-glycine, rotamer population p_I correlates with the longest fluorescent decay, p_{II} correlates with the shortest decay time, and p_{III} correlates with an intermediate decay time.

Gauduchon and Wahl⁽²⁾ and Ross and Laws⁽⁵⁾ proposed that the fluorescence decay times of individual rotamer populations are a consequence of different quenching routes relating to the proximity of the electron withdrawing and donating peptidic groups. In order to test this idea, we measured the fluorescence decays of YA in a series of acetonitrile/water mixtures of varying polarity. If electron-transfer quenching occurs, we expected to observe systematic changes in quenching with solvent polarity as a result of changing the driving force for electron transfer ($-\Delta G_{et}^{\circ}$). Figure 5 depicts changes in the quenching rate of tyrosine as a function of solvent polarity. The change in quenching rate was determined with the following equation:

$$\Delta k_{et} = [(1/\tau_i) - (1/\tau_{ref})] \quad (5)$$

where τ_i is the fluorescence decay time in a given solvent and τ_{ref} is the fluorescence decay time of reference determined when the YA is dissolved in 100% acetonitrile. Solvent polarity is quantified in Fig. 5 by the empirical

Table II. Quantum Yield Values for Tyrosine

Solvent	Conc.	Temp. (°C)	Quantum yield	Source
pH 7	0.3 mM	25	~0.07	This work
pH 6	10^{-4} – 10^{-5} M	23	0.14 ± 0.01	[35]
pH 6-7	—	22–24	0.04	[18]
—	10^{-5} M	—	0.21	[17]
—	—	—	0.088	[28]

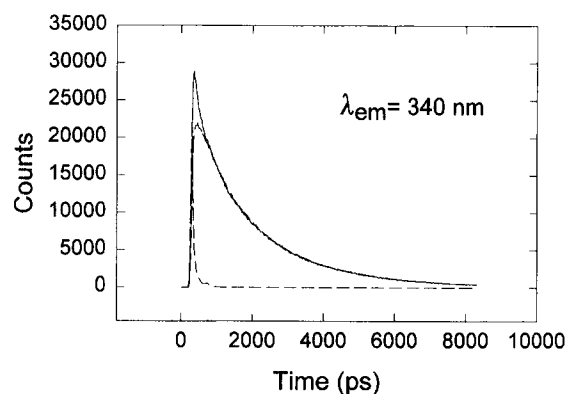
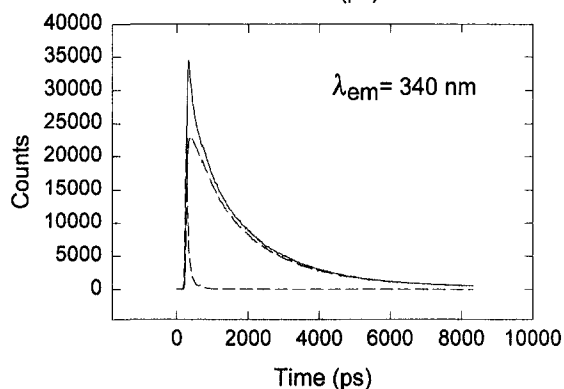
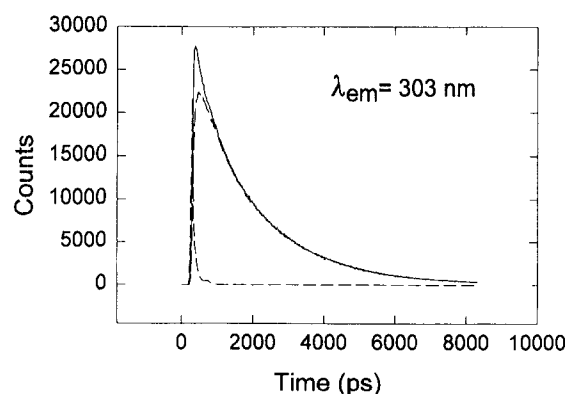
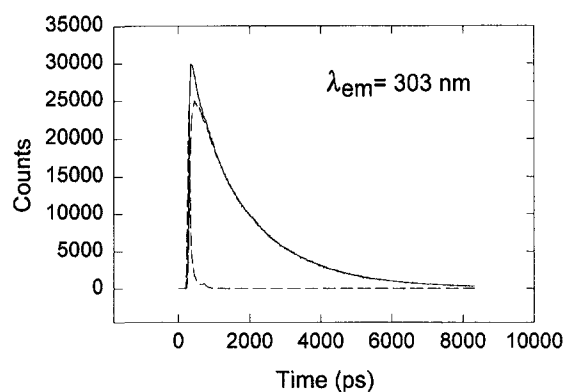


Fig. 3. Fluorescence decay of the tyrosine–alanine dipeptide at 303 nm (top) and 340 nm (bottom) with excitation at 287 nm. Decays are shown for fluorescence polarized parallel (top curve) and perpendicular (bottom curve) to the excitation polarization. Fluorescence intensity and anisotropy decay parameters are given in Table III.

Fig. 4. Fluorescence decay of the tyrosine–leucine dipeptide at 303 nm (top) and 340 nm (bottom) with excitation at 287 nm. Decays are shown for fluorescence polarized parallel (top curve) and perpendicular (bottom curve) to the excitation polarization. Fluorescence intensity and anisotropy decay parameters are given in Table III.

E_T (30) parameter,⁽²⁹⁾ which measures the effect of solvent on the transition energy of a solvatochromic dye having a large ground-state transition dipole. Another variable in the data presented in Fig. 5 is the concentration of hydrogen bond donors and acceptors. However, H-bonding is expected to lead to a red shift in the fluorescence emission⁽²⁶⁾ and therefore probably does not contribute much to the fluorescence detected at 303 nm.

The variation in quenching rate with solvent polarity evidenced in Fig. 5 supports the idea that quenching occurs by charge transfer. As the polarity is increased, the energy of the charge-transfer state generated by quenching is expected to be lowered, increasing the driving force for electron transfer. The fact that the quenching rate increases with increased driving force shows that electron transfer occurs in the normal (rather than

Table III. Analysis of Dipeptide Fluorescence Decays

Sample	λ_{em}	a_1	a_2	a_3	τ_1 (ns)	τ_2 (ns)	τ_3 (ns)	r_0	τ_{rot} (ps)	χ^2
YA ^a	303	0.70	0.30		1.80	0.45		0.32	47	2.2
YA	303	0.45	0.33	0.22	2.00	0.10	0.79	0.32	47	1.6
YA	340	0.49	0.51		2.20	0.56		0.30	63	2.2
YL ^b	303	0.63	0.37		1.90	0.46		0.28	60	2.2
YL	340	0.60	0.40		2.00	0.45		0.26	75	2.2

Rotamer populations determined by NMR

	P_I	P_{II}	P_{III}
YA	0.47	0.33	0.20

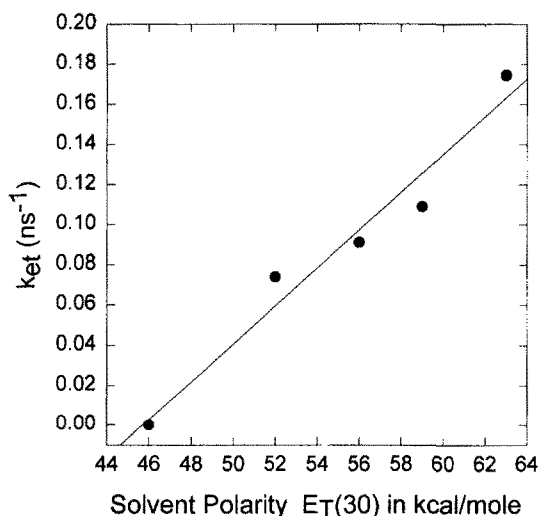
^a Tyrosine–alanine.^b Tyrosine–leucine.

Fig. 5. Change in the fluorescence decay rate with solvent polarity. The change was determined relative to the fluorescence decay in acetonitrile. Solvent polarity is characterized by the $E_T(30)$ parameter (see text).

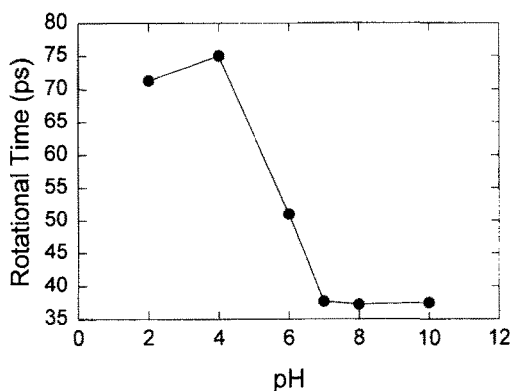


Fig. 6. Dependence of the rotational correlation time of tyrosine on pH. Tyrosine emission was measured at 303 nm.

the Marcus inverted) regime.⁽³⁰⁾ If we assume that the change in driving force is roughly linear in polarity, then the approximately linear dependence on E_T ⁽³⁰⁾ implies the existence of a linear free energy relationship between quenching rate and driving force.⁽²⁹⁾ Such a relationship follows from Marcus theory of electron transfer in the limit where the relative change in driving force induced by changes in polarity is small.

Fluorescence Anisotropy Decays

Rotational correlation times, obtained from fits to fluorescence anisotropy decays, are a potentially rich source of information about interactions with the environment and peptide conformational dynamics. Hence, it is important to understand anisotropy decays detected in tyrosyl fluorescence. For tyrosine at pH 7, a single rotational time of 36 ± 5 ps was measured with an initial anisotropy of 0.27 ± 0.02 . These values are identical within experimental error to values obtained by Lakowicz and co-workers for tyrosine and *N*-acetyltyrosinamide^(3,4) by frequency-domain phase modulation fluorometry and quenching-dependent anisotropy measurements. An initial anisotropy of 0.30 ± 0.01 was measured for tyrosine in 70% glycerol, comparable to values obtained by frequency domain⁽³⁾ and streak camera measurements.⁽³¹⁾

The rotational time increases at lower pH values, as shown in Fig. 6, suggesting an enhanced interaction of tyrosine with the solvent at lower pH. The increased rotational time could result from the formation of a charged (rather than zwitterionic) species, which might result in interaction with a cloud of negative charges. Another possibility is the formation of a complex at low pH, effectively increasing the size of the rotating species.

Rotational correlation times are given in the hydrodynamic limit by Stokes–Einstein–Debye (SED) theory. The SED equation is

$$\tau_r = \frac{\eta V}{kT} F \quad (6)$$

where η is the solvent viscosity, V is the volume, and F is a correction that depends on shape and coupling to the solvent.⁽³²⁾ Figure 7 depicts the dependence of the rotational time of tyrosine in solutions of different viscosity. The rotational correlation time is linear over a wide range of viscosities, with a slope of 44 ± 1 ps/cP. This viscosity dependence is close to the SED prediction of 51 ps/cP for “stick” boundary conditions and a spherical shape ($F = 1$), given a tyrosine volume (205

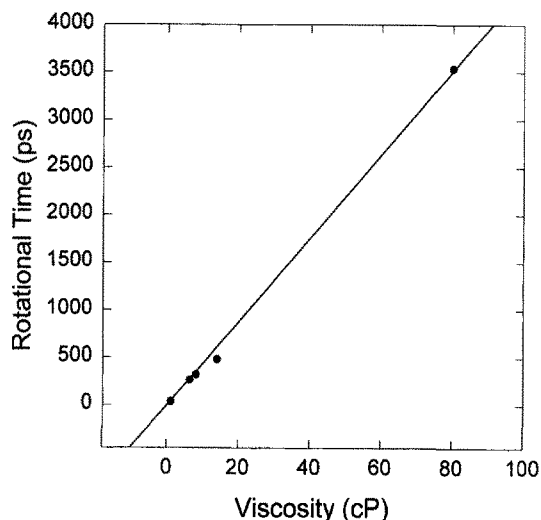


Fig. 7. Viscosity dependence of the rotational correlation of tyrosine. The solvents used were, in order of increasing viscosity, water, ethylene glycol/water, propylene glycol/water, and glycerol/water. The line shows a linear regression fit to the data with a slope of 44 ps/cP.

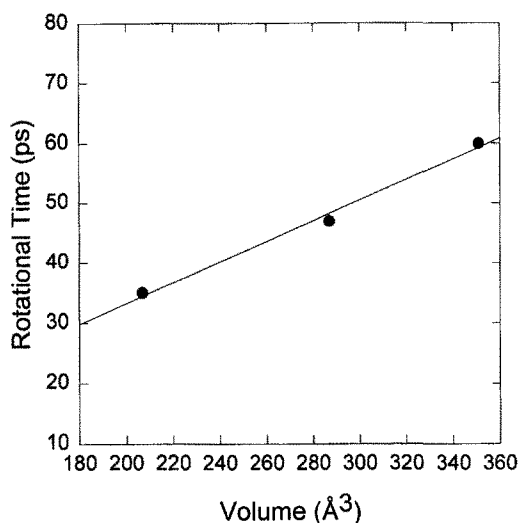


Fig. 8. Dependence of rotational correlation times on volume for tyrosine, tyrosine-alanine, and tyrosine-leucine. Volumes were estimated from the van der Waals volumes by molecular modeling (see text). The solid line shows a linear regression fit with a slope of 0.17 ps/Å³.

Å³) estimated from van der Waals volumes in the molecular modeling program CHARMM. Approximate agreement with SED predictions with sticking boundary conditions has been noted previously for solutes in water and indicates strong interaction with the solvent.⁽³³⁾

Both the increased rotational time and the lower initial anisotropy associated with the emission at 340 nm show that a distinct species is responsible for this emission. The increased rotational time associated with the 340-nm emission relative to the rotational time obtained with 303-nm emission could indicate either increased friction or increased size. Slower rotation is likely the result of a hydrogen-bonding interaction of the phenol group with a phosphate or with the aqueous solvent. Increased friction due to ionic and hydrogen-bonding interactions has been observed previously for polar and hydrogen-bonding solvents.^(33,34) A strong hydrogen-bonding interaction could also effectively increase the size of the rotating species.

The YA and YL dipeptides exhibit longer rotational correlation times (see Table III) than the tyrosine monomer, as expected based on their increased size. A similar value was reported by Lakowicz and Maliwal⁽³⁾ for the tyrosine-tyrosine dipeptide. As in the tyrosine monomer, the rotational diffusion times of the dipeptides increase significantly for emission at 340 nm. In all cases a single rotational correlation time was found to be sufficient, and a significant improvement in χ_r^2 was not found with two anisotropy decay components.

Figure 8 shows the relationship between the rotational correlation time and the volume (as calculated in the CHARMM molecular modeling program) for tyrosine, YA, and YL. A linear dependence of rotation on volume is predicted by the SED equation [Eq. (5)]. The slope in Fig. 8 is about 70% of that predicted by the SED equation for a spherical rotor with stick boundary conditions. This deviation could result from a number of factors that are difficult to quantify without knowledge of the actual structure of the rotating species. These factors include (a) the shape, which alters the coupling to the solvent;⁽³²⁾ (b) the orientation of the emission dipole moment with respect to the principal diffusion axes; and (c) the volume, which may not be accurately predicted by van der Waals radii. Nevertheless, the dependence in Fig. 8 shows that the rotational relaxation of these species is at least semiquantitatively in agreement with predictions based on the hydrodynamic SED equation.

The use of the SED equation to describe the rotational correlation times of tyrosine and dipeptides merits comment. The SED equation is strictly valid for rigid molecules, whereas the species probed here possess internal degrees of freedom, for example, interconversion of rotamers, that might conceivably contribute to the anisotropy decay. We find no evidence, for example, in the form of multiexponential anisotropy decays, that internal

motions contribute to the observed anisotropy decays. This is not surprising, because such motions are likely to occur on time scales longer than the fluorescence lifetime. For example, the correlation of the rotamer populations determined by NMR with the fluorescence decay amplitudes shows that dipeptide rotamer populations do not interconvert on the time scale of the fluorescence decay and, *a fortiori*, cannot contribute to the anisotropy decay. Local tyrosyl motions in dipeptides, however, would probably not be detectable since the time scale of these motions, if estimated to be similar to the rotational correlation time of tyrosine itself (*ca.* 38 ps), would not be resolvable from the rotational diffusion of the dipeptides.

CONCLUSIONS

The present study demonstrates that time-resolved tyrosine fluorescence measurements can serve as a valuable intrinsic probe in peptides containing a single tyrosyl residue. The TCSPC technique used here provides measurements that accord with results obtained by other techniques, such as frequency-domain fluorometry.^(3,4) The rotamer model^(2,5,10) can account for the multiexponential fluorescence decays observed in the tyrosine-alanine and tyrosine-leucine dipeptides. The fact that fluorescence quenching is enhanced with increasing polarity of the environment strongly supports the previously proposed charge-transfer mechanism of quenching.

Rotational correlation times, which provide information about the strength of interaction of the solute with the solution, show that emission at 303 and 340 nm from tyrosine solutions results from two distinct species with different rotational correlation times. The initial anisotropy $r(0)$ of tyrosine, 0.30 ± 0.02 , is sufficiently high for measurement of rotational relaxation measurements of tyrosine. Measurements of the rotational correlation time can be used to probe interactions with the solvent and to estimate the volume of the fluorescing species. We expect that rotational correlation times will be a valuable diagnostic tool for biomolecules in solution, both for identifying the emitting species and for probing their interaction with the environment. Tyrosine and tyrosyl peptides follow hydrodynamic (Stokes-Einstein-Debye) predictions near pH 7. However, at more acidic and more basic pH levels the rotation time is longer, possibly due to ionic friction or association with the solvent.

ACKNOWLEDGMENTS

We wish to thank Prof. Graham Fleming and Dr. Gary Holtom for graciously sharing their TCSPC fitting programs with us. J. F. H. was supported in part by an NSF Macro ROA grant. This work was supported by NSF EPSCoR Grant No. OSR-9255223 and by University of Kansas General Research allocation No. 3808.

REFERENCES

1. J. R. Lakowicz (Ed.) (1991–1997) *Topics in Fluorescence Spectroscopy, Vols. 1–5*, Plenum Press, New York.
2. P. Gauduchon and P. Wahl (1978) *Biophys. Chem.* **8**, 87–104.
3. J. R. Lakowicz and B. P. Maliwal (1983) *J. Biol. Chem.* **258**, 4794–4801.
4. J. R. Lakowicz, G. Laczko, and I. Gryczynski (1987) *Biochemistry* **26**, 82–90.
5. J. B. A. Ross, W. R. Laws, A. Buku, J. C. Sutherland, and H. R. Wyssbrod (1986) *Biochemistry* **25**, 608–612.
6. H. Pal, D. K. Palit, T. Mukherjee, and J. P. Mittal (1990) *J. Photochem. Photobiol. A* **52**, 391–409.
7. J. B. A. Ross, W. R. Laws, K. W. Rousslang, and H. R. Wyssbrod (1992) in *Topics in Fluorescence Spectroscopy, Vol. 3*, J. R. Lakowicz (Ed.), Plenum Press, New York, pp. 1–63.
8. J. R. Lakowicz, B. Kierdaszuk, P. Callis, H. Malak, and I. Gryczynski (1995) *Biophys. Chem.* **56**, 263–271.
9. G. Weber (1960) *Biochem. J.* **75**, 335–345.
10. W. R. Laws, J. B. A. Ross, H. R. Wyssbrod, J. M. Beechem, L. Brand, and J. C. Sutherland (1986) *Biochemistry* **25**, 599–607.
11. R. Schwarzwald, C. Seidel, R. S. Goody, K. P. Kühn, and K.-O. Greulich (1989) *Ber. Bunsenges. Phys. Chem.* **93**, 342–346.
12. R. Schwarzwald and K.-O. Greulich (1988) *Ber. Bunsenges. Phys. Chem.* **92**, 447–450.
13. J. B. A. Ross, W. R. Laws, J. C. Sutherland, A. Buku, P. G. Katsoyannis, I. L. Schwartz, and H. R. Wyssbrod (1986) *Photochem. Photobiol.* **44**, 365–370.
14. R. W. Cowgill (1967) *Biochim. Biophys. Acta* **133**, 6–18.
15. R. W. Cowgill (1976) in *Biochemical Fluorescence Concepts, Vol. 2*, R. F. Chen and H. Edelhoch (Eds.), Marcel Dekker, New York, pp. 441–486.
16. C. Seidel, A. Orth, and K.-O. Greulich (1993) *Photochem. Photobiol.* **58**, 178–184.
17. F. W. J. Teale and G. Weber (1957) *Biochem. J.* **65**, 476–482.
18. V. G. Shore and A. B. Pardee (1956) *Arch. Biochem. Biophys.* **60**, 100–107.
19. G. S. Harms, S. W. Pauls, J. F. Hedstrom, and C. K. Johnson (1997) *J. Fluoresc.* **7**, 283–292.
20. G. R. Holtom (1990) *Proc. SPIE* **1204**, 1–12.
21. A. J. Cross and G. R. Fleming (1984) *Biophys. J.* **46**, 45–56.
22. S. J. Strickler and R. A. Berg (1962) *J. Chem. Phys.* **37**, 814–822.
23. J. B. Birks and D. J. Dyson (1963) *Proc. R. Soc. London Ser. A* **275**, 135–148.
24. National Research Council (U.S.) (1926) *International Critical Tables of Numerical Data, Physics, Chemistry and Technology*, McGraw-Hill, New York.
25. H. Langhals (1982) *Angew. Chem. Int. Ed. Engl.* **21**, 724–733.
26. K. J. Willis and A. G. Szabo (1991) *J. Phys. Chem.* **95**, 1585–1589.
27. G. Weber (1960) *Biochem. J.* **75**, 345–352.
28. H. C. Borresen (1967) *Acta Chem. Scand.* **21**, 920–936.
29. C. Reichardt (1988) *Solvents and Solvent Effects in Organic Chemistry*, 2nd ed., VCH, Weinheim, Germany.

30. R. A. Marcus and N. Sutin (1985) *Biochim. Biophys. Acta* **811**, 265–322.
31. X.-Y. Liu and T. M. Nordlund (1990) *Proc. SPIE Int. Soc. Opt. Eng.* **1204**, 669–675.
32. C. R. Cantor and P. R. Schimmel (1980) *Biophysical Chemistry*, W. H. Freeman, New York, Vol. II.
33. A. M. Williams, Y. Jiang, and D. Ben-Amotz (1994) *Chem. Phys.* **180**, 119–129.
34. N. Balabai and D. H. Waldeck (1997) *J. Phys. Chem. B* **101**, 2339–2347.
35. R. F. Chen (1967) *Anal. Lett.* **1**, 35–42.